An efficient non-linear polynomial color characterization method based on interrelations of color spaces

Journal:	*Color Research and Application*
Manuscript ID	COL-19-119.R2
Wiley - Manuscript type:	Research Article
Date Submitted by the Author:	n/a
Complete List of Authors:	ji, jing; Xi'an Jiaotong University, State Key Laboratory of Manufacturing Systems Engineering, Xi'an 710049, China; Xi'an Jiaotong University Museum, Xi'an Jiaotong University, Xi'an 710049, China Fang, Suping Shi, Zhengyuan; School of Mathematics and Statistics, Xi'an Jiaotong University, Xi'an 710049, China Xia, Qing; School of Mathematics and Statistics, Xi'an Jiaotong University, Xi'an 710049, China Li, Yibao; School of Mathematics and Statistics, Xi'an Jiaotong University, Xi'an 710049, China
Keywords:	Color correction, Color characterization, Non-linear transformation, Polynomial regression

An efficient non-linear polynomial color characterization method based on interrelations of color spaces

Jing Ji[a,b], Suping Fang[a,*], Zhengyuan Shi[c], Qing Xia[c], Yibao Li[c]

[a] *Xi'an Jiaotong University, State Key Laboratory of Manufacturing Systems Engineering, Xi'an 710049, China*
[b] *Xi'an Jiaotong University Museum, Xi'an Jiaotong University, Xi'an 710049, China*
[c] *School of Mathematics and Statistics, Xi'an Jiaotong University, Xi'an 710049, China*

Abstract

A well-known color characterization method is to take an image of a color chart and then to find the mapping matrix from the digital RGBs to the corresponding known CIEXYZs. However, the prediction errors are generally large in CIELAB color space because of the nonlinear transformation from CIEXYZs to CIELABs. In this paper, we propose an efficient and simple non-linear method for the color characterization of input devices. The approach for deriving a colorimetric mapping between digital RGB signals and CIELAB tristimulus values uses the polynomial modeling by considering the interrelations among the standard CIE color spaces. Furthermore, to improve the accuracy of solution, we take the polynomial root terms extension. Our algorithm is simple to implement because only a least-squares mapping should be solved. Various computational results are given to demonstrate the efficiency and capability of the proposed method.

Keywords: Color correction; Color characterization; Non-linear transformation; Polynomial regression

1. Introdution

Digital camera is an effective device to record color information with pixel accuracy. It is widely applied in color reproduction without contacting the objects, especially in cultural relics high-fidelity digital reproduction[1, 2, 3]. However, the images captured by cameras rely on devices and light source. RGB responses of the same image is different by different filming conditions, which severely limits the application of cameras in color reproduction. Therefore, RGB information captured by the camera needs to be converted to a standard color space independent of interfering factors. This process is called color characterization [4].

Typical color characterization methods include three-dimensional look-up table method with interpolation and extrapolation [5, 6], polynomial modeling method [7], and neural network [8]. For the look-up table method, a large training set is necessary as proposed in [9]. The method of neural network can produce good effects in nonlinear mapping, but its processing speed is low and a lot of samples are needed [10, 11]. Comparing with the previous methods, the polynomial modeling method is more practical and efficient

*Correspondence to: Suping Fang (e-mail: spfang@mail.xjtu.edu.cn)

which only needs a reference target with a certain number of color samples. Kang [7] transformed digital RGB values preprocessed by grey balance to CIEXYZ color space using polynomial regression. The author summarized that the fitting accuracy of training data is improved and the accuracy of testing data may be worse as the order of polynomials increasing. Hong et al.[12, 13] used different polynomials and 8-bit and 12-bit digital RGB data to test the accuracy of color characterization. They also compared the color characterization performance between the high-end and low-end digital cameras and pointed out the range of possibilities for improving the accuracy of color characterization. Hardeberg [14, 15] introduced a preprocess of polynomial regression in which a cubic root of RGB values was used. Andersen et al.[16] proposed a method called Hue Plane Preserving Color Correction(HPPCC) which matches digital RGBs to CIEXYZs in each hue slice of color space with different polynomial transformations. Huang et al.[17] improved the polynomial modeling by replacing the inherent camera RGB values with normalized luminance. Finlayson et al.[18] proposed the white preserving color correction which is well-behaved when the training set is incomplete. However, this method may result in a higher mean error than conventional color correction while exactly matching the white patch. After that, they proposed root-polynomial color correction related to the idea of fractional polynomials[19]. In the above research, the polynomial regression was used to transform digital RGB values to CIEXYZ values. However, as the CIEXYZ space is an non-uniform color space, the minimized error obtained by regression algorithm in the CIEXYZ space is poorly correlated to visual color differences, thus leading to unsatisfactory results.

In this paper, we set a polynomial regression model using CIELAB space as the destination color space, because Euclidean distance in this space can evaluate perceptual color differences quite well. The main contribution of this paper is to improve the accuracy of color characterization through the following two aspects: First, comparing with the previous related studies [14, 20], our proposed method considers the interrelation among the standard CIE color spaces and presents a complete theoretical derivation form the device-dependent color space to the standard CIELAB space. Second, the polynomial root terms extension is constructed in our proposed method to further improve the transformation accuracy. To avoid misunderstanding, we have to point that our method is not exposure invariant (as mentioned in [19]) due to the nonlinear transformation from digital RGB values to CIELAB values. Various tests have been performed to verify the performance of the proposed method at the same exposure level.

The rest of this paper is organized as follows: The background of polynomial approach on color characterization is presented in Section 2. Our method is drawn in Section 3. The experiments are presented in Section 4. The conclusion is given in Section 5.

2. Problem Formulation And Related Works

2.1. Polynomial color characterization

A color chart with a set of n color samples is scanned. For each color sample, the corresponding tristimulus value is known and defined as a three dimensional vector $\boldsymbol{q}$ ($\boldsymbol{q} \in \mathbb{R}^{3\times 1}$) and the device three dimensional digital response is defined as $\boldsymbol{\rho}$ ($\boldsymbol{\rho} \in \mathbb{R}^{3\times 1}$). A simple linear color characterization transformation can be written as follows:

$$\boldsymbol{M} \cdot \boldsymbol{\rho} = \boldsymbol{q}. \tag{1}$$

Vector $\boldsymbol{\rho}$ can be extended to m dimensions by increasing basis function in polynomial regression. For the 1st, 2nd, 3rd and 4th order polynomial expansions, vector $\boldsymbol{\rho}$ is depicted by $\boldsymbol{\rho}_k (k = 1, 2, 3, 4)$ as

$$\begin{cases} \boldsymbol{\rho}_1(r,g,b) = \left(1, r, g, b\right)^T \\ \boldsymbol{\rho}_2(r,g,b) = \left(1, r, g, b, r^2, g^2, b^2, rg, rb, gb\right)^T \\ \boldsymbol{\rho}_3(r,g,b) = \left(1, r, g, b, r^2, g^2, b^2, rg, rb, gb, r^3, g^3, b^3, rg^2, r^2g, gb^2, g^2b, rb^2, r^2b, rgb\right)^T \\ \boldsymbol{\rho}_4(r,g,b) = \left(1, r, g, b, r^2, g^2, b^2, rg, rb, gb, r^3, g^3, b^3, rg^2, r^2g, gb^2, g^2b, rb^2, r^2b, rgb, r^4, \right. \\ \qquad\qquad \left. g^4, b^4, gr^3, br^3, rg^3, bg^3, rb^3, gb^3, gbr^2, rbg^2, rgb^2, r^2g^2, r^2b^2, b^2g^2\right)^T \end{cases}$$

We define $\boldsymbol{P}$ ($\boldsymbol{P} \in \mathbb{R}^{m\times n}, m \ll n$) as a $m \times n$ matrix of vector $\boldsymbol{\rho}$ and $\boldsymbol{Q}$ ($\boldsymbol{Q} \in \mathbb{R}^{3\times n}$) as the corresponding matrix of vector $\boldsymbol{q}$. The mapping relationship between the camera response space and the corresponding tristimulus value space can be represented by

$$\boldsymbol{M} \cdot \boldsymbol{P} = \boldsymbol{Q}, \tag{2}$$

where $\boldsymbol{M}$ is the mapping matrix that depends on $\boldsymbol{P}$ and $\boldsymbol{Q}$. The key of color characterization is to find the optimal mapping matrix $\boldsymbol{M}$.

2.2. Color space conversion formula

The CIE 1931 Standard RGB Colorimetric System(CIERGB), a basis in colorimetry, is a linear transformation of the CIE 1931 Standard XYZ Colorimetric System(CIEXYZ) as

$$\begin{bmatrix} X \\ Y \\ Z \end{bmatrix} = \boldsymbol{A} \cdot \begin{bmatrix} R \\ G \\ B \end{bmatrix}, \tag{3}$$

where $\boldsymbol{A}$ is

$$\boldsymbol{A} = \begin{bmatrix} 2.7689 & 1.7517 & 1.1302 \\ 1.0000 & 4.5907 & 0.0601 \\ 0.0000 & 0.0565 & 5.5943 \end{bmatrix}. \tag{4}$$

The CIELAB space is an uniform color space for practical applications, which is defined by the quantities L, a and b. The relationship between CIELAB and CIEXYZ is defined as follows:

$$\begin{cases} L = 116 f\left(\frac{Y}{Y_n}\right) - 16 \\ a = 500\left[f\left(\frac{X}{X_n}\right) - f\left(\frac{Y}{Y_n}\right)\right] \\ b = 200\left[f\left(\frac{Y}{Y_n}\right) - f\left(\frac{Z}{Z_n}\right)\right] \end{cases} \tag{5}$$

where

$$f(a) = \begin{cases} a^{\frac{1}{3}} & \text{if} \quad a \geq 0.008856 \\ 7.787a + \frac{16}{116} & \text{otherwise.} \end{cases} \tag{6}$$

It should be pointed that $f(a)$ can be simplified as $f(a) = a^{\frac{1}{3}}$, because $7.787a + 16/116 \approx a^{\frac{1}{3}}$, if $a < 0.008856$. X_n, Y_n and Z_n denote the tristimulus values of nominally white stimulus. A widely used method comparing two colors denoted by $[L_1, a_1, b_1]$ and $[L_2, a_2, b_2]$ is to calculate the Euclidean distance in CIELAB space as

$$\Delta E_{ab} = \sqrt{(L_1 - L_2)^2 + (a_1 - a_2)^2 + (b_1 - b_2)^2}. \tag{7}$$

As the evaluation criteria proposed in [21], if $\Delta E_{ab} \in [0 \;\; 3]$, the quality of color characterization is very good. If $\Delta E_{ab} \in (3 \;\; 6]$, its quality is good. If $\Delta E_{ab} \in (6 \;\; 10]$, its quality is sufficient. Otherwise, its quality is insufficient.

2.3. Classic color characterization models.

The relationship between source color space and destination color space is presented in Fig. 1(a). Several classic color characterization model are available based on model-transformation methods and the destination color space.

Fig. 1(b) shows the polynomial regression to CIEXYZ space [12]. The digital RGB values are transformed to CIEXYZ values by polynomial regression. And then CIELAB values can be derived from CIEXYZ values by a standardized formula which has been illustrated in Eq. (5).

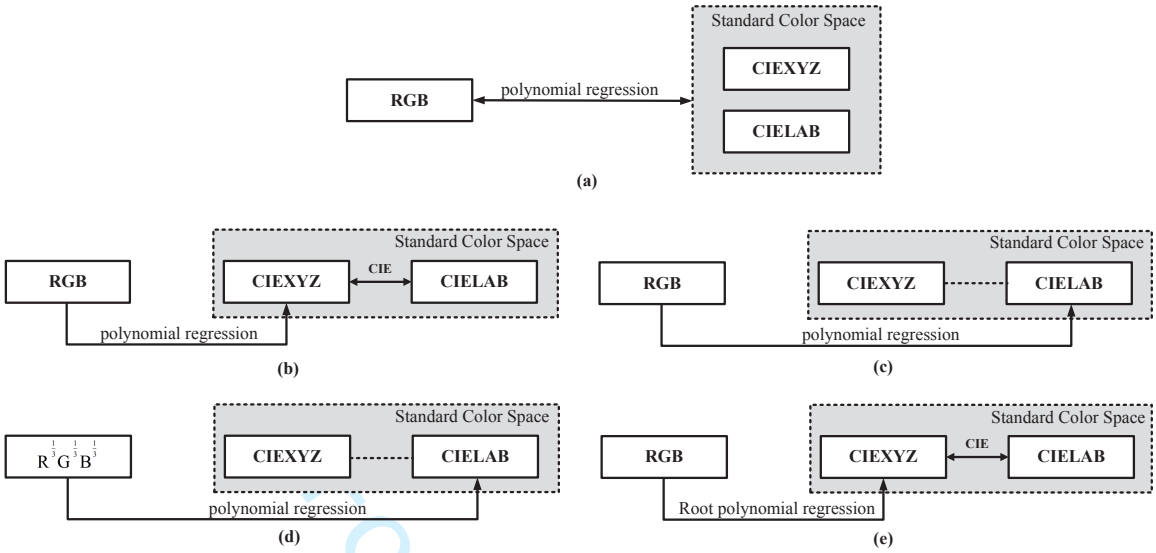

Figure 1: Classic color characterization models.

Fig. 1(c) shows the polynomial regression to CIELAB space [20]. It is clear that the relationship between digital RGB values and CIELAB values is nonlinear. Therefore, n-order polynomial regression is used to model the transformation.

Fig. 1(d) shows Hardeberg's Method [14] which applied a non-linear correction to the digital RGB values before polynomial regression in the form of cubic squares. Here $\boldsymbol{\rho}_k(r,g,b)$ are replaced by $\boldsymbol{\rho}_k(r^{\frac{1}{3}},g^{\frac{1}{3}},b^{\frac{1}{3}})$.

Finlayson's method [19] aims to find the root-polynomial expansions (RPCC) of all k-order polynomial as shown in Fig. 1(e). The root-polynomial expansions $\boldsymbol{\rho}_k(k=1,2,3,4)$ are given below:

$$\begin{cases} \boldsymbol{\rho}_1 = (r,g,b)^T \\ \boldsymbol{\rho}_2 = (r,g,b,\sqrt{rg},\sqrt{gb},\sqrt{rb})^T \\ \boldsymbol{\rho}_3 = (r,g,b,\sqrt{rg},\sqrt{gb},\sqrt{rb},\sqrt[3]{rg^2},\sqrt[3]{gb^2},\sqrt[3]{rb^2},\sqrt[3]{gr^2},\sqrt[3]{bg^2},\sqrt[3]{br^2},\sqrt[3]{rgb})^T \\ \boldsymbol{\rho}_4 = (r,g,b,\sqrt{rg},\sqrt{gb},\sqrt{rb},\sqrt[3]{rg^2},\sqrt[3]{gb^2},\sqrt[3]{rb^2},\sqrt[3]{gr^2},\sqrt[3]{bg^2},\sqrt[3]{br^2},\sqrt[3]{rgb} \\ \qquad \sqrt[4]{r^3g},\sqrt[4]{r^3b},\sqrt[4]{g^3r},\sqrt[4]{g^3b},\sqrt[4]{b^3r},\sqrt[4]{b^3g},\sqrt[4]{r^2gb},\sqrt[4]{g^2rb},\sqrt[4]{b^2rg})^T \end{cases}$$

In this method, the root polynomial regression is applied to transform digital RGB values to CIEXYZ values, then CIELAB values and color differences are obtained in Section 2.2.

3. The Proposed Method

The schematic of our proposed method is shown in Fig. 2. In our method, by analyzing the relationship among the standard color space(CIERGB, CIEXYZ and CIELAB), we first construct the mapping relationship from the device RGB space to CIELAB color space based on backward-deduction method in Section

3.1. And then, in order to further improve the transformation accuracy, the high order extension polynomial method is introduced in Section 3.2.

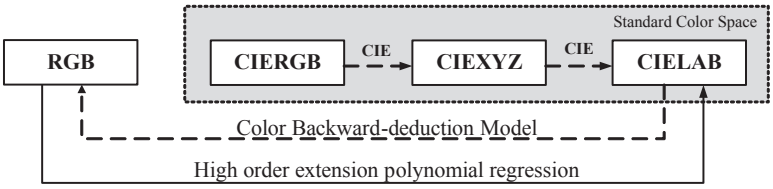

Figure 2: Schematic of our proposed method.

3.1. Mapping relationship between device RGB space and CIELAB space

It is generally known that the color difference in CIELAB space is used to evaluate the accuracy of color characterization method. So we need to map digital RGB values to CIELAB values through a series of transformations. It is easy to establish a relationship between CIERGB and CIEXYZ because of the linear transformation as shown in Eq. (3). However, the relationship between CIEXYZ and CIELAB is nonlinear, which involves a cubic relevance. According to the standardized formula among CIE standard color values given in Section 2.2, Eq. (5) can be transformed into multidimensional form

$$[L,a,b]^T = \boldsymbol{N} \times \left[f\left(\frac{X}{X_n}\right), f\left(\frac{Y}{Y_n}\right), f\left(\frac{Z}{Z_n}\right) \right]^T + \boldsymbol{V}, \tag{8}$$

where

$$\boldsymbol{N} = \begin{bmatrix} 0 & 116 & 0 \\ 500 & -500 & 0 \\ 0 & 200 & -200 \end{bmatrix} \quad \text{and} \quad \boldsymbol{V} = [\ -16 \quad 0 \quad 0\ ]^T. \tag{9}$$

Because of Eq. (3), we have

$$\begin{bmatrix} X \\ Y \\ Z \end{bmatrix} = \begin{bmatrix} 2.7689 & 1.7517 & 1.1302 \\ 1.0000 & 4.5907 & 0.0601 \\ 0.0000 & 0.0565 & 5.5943 \end{bmatrix} \begin{bmatrix} R \\ G \\ B \end{bmatrix} \Leftrightarrow \begin{bmatrix} \frac{X}{X_n} \\ \frac{Y}{Y_n} \\ \frac{Z}{Z_n} \end{bmatrix} = \begin{bmatrix} \frac{2.7689}{X_n} & \frac{1.7517}{X_n} & \frac{1.1302}{X_n} \\ \frac{1.0000}{Y_n} & \frac{4.5907}{Y_n} & \frac{0.0601}{Y_n} \\ 0.0000 & \frac{0.0565}{Z_n} & \frac{5.5943}{Z_n} \end{bmatrix} \begin{bmatrix} R \\ G \\ B \end{bmatrix} \tag{10}$$

Furthermore, we have

$$\begin{cases} f\left(\frac{X}{X_n}\right) & = \left(\frac{X}{X_n}\right)^{\frac{1}{3}} & = \left(\frac{2.7689}{X_n}R + \frac{1.7517}{X_n}G + \frac{1.1302}{X_n}B\right)^{\frac{1}{3}} \\ f\left(\frac{Y}{Y_n}\right) & = \left(\frac{Y}{Y_n}\right)^{\frac{1}{3}} & = \left(\frac{1.0000}{Y_n}R + \frac{4.5907}{Y_n}G + \frac{0.0601}{Y_n}B\right)^{\frac{1}{3}} \\ f\left(\frac{Z}{Z_n}\right) & = \left(\frac{Z}{Z_n}\right)^{\frac{1}{3}} & = \left(\frac{0.0000}{Z_n}R + \frac{0.0565}{Z_n}G + \frac{5.5943}{Z_n}B\right)^{\frac{1}{3}} \end{cases} \tag{11}$$

Then, we assume there exits the new vector $[(r^*)^{\frac{1}{3}},\ (g^*)^{\frac{1}{3}},\ (b^*)^{\frac{1}{3}}]^T$, which satisfies

$$\begin{bmatrix} f\left(\frac{X}{X_n}\right) \\ f\left(\frac{Y}{Y_n}\right) \\ f\left(\frac{Z}{Z_n}\right) \end{bmatrix} = \begin{bmatrix} \left(\frac{2.7689}{X_n}\right)^{\frac{1}{3}} & \left(\frac{1.7517}{X_n}\right)^{\frac{1}{3}} & \left(\frac{1.1302}{X_n}\right)^{\frac{1}{3}} \\ \left(\frac{1.0000}{Y_n}\right)^{\frac{1}{3}} & \left(\frac{4.5907}{Y_n}\right)^{\frac{1}{3}} & \left(\frac{0.0601}{Y_n}\right)^{\frac{1}{3}} \\ 0.0000 & \left(\frac{0.0565}{Z_n}\right)^{\frac{1}{3}} & \left(\frac{5.5943}{Z_n}\right)^{\frac{1}{3}} \end{bmatrix} \begin{bmatrix} (r^*)^{\frac{1}{3}} \\ (g^*)^{\frac{1}{3}} \\ (b^*)^{\frac{1}{3}} \end{bmatrix} \tag{12}$$

Here a color characterization transformation is assumed as

$$\left[(r^*)^{\frac{1}{3}},\ (g^*)^{\frac{1}{3}},\ (b^*)^{\frac{1}{3}}\right]^T = \hat{\boldsymbol{M}} \cdot \hat{\boldsymbol{\rho}}(R^{\frac{1}{3}},\ G^{\frac{1}{3}},\ B^{\frac{1}{3}}), \tag{13}$$

where $\hat{\boldsymbol{M}}$ is the mapping matrix that depneds Eqs. (11) and (12) and $\hat{\boldsymbol{\rho}}$ is a polynomial regression. Since digital RGB values are transformed to CIERGB values by polynomial regression and the matrix $\check{\boldsymbol{M}}$, we can get

$$\hat{\boldsymbol{\rho}}(R^{\frac{1}{3}},\ G^{\frac{1}{3}},\ B^{\frac{1}{3}}) = \check{\boldsymbol{M}} \cdot \boldsymbol{\rho}(r^{\frac{1}{3}},\ g^{\frac{1}{3}},\ b^{\frac{1}{3}}). \tag{14}$$

The key to color characterization is to find the optimal mapping matrix $\boldsymbol{M} = \hat{\boldsymbol{M}} \cdot \check{\boldsymbol{M}}$. By assuming

$$\boldsymbol{A}^* = \begin{bmatrix} \left(\frac{2.7689}{X_n}\right)^{\frac{1}{3}} & \left(\frac{1.7517}{X_n}\right)^{\frac{1}{3}} & \left(\frac{1.1302}{X_n}\right)^{\frac{1}{3}} \\ \left(\frac{1.0000}{Y_n}\right)^{\frac{1}{3}} & \left(\frac{4.5907}{Y_n}\right)^{\frac{1}{3}} & \left(\frac{0.0601}{Y_n}\right)^{\frac{1}{3}} \\ 0.0000 & \left(\frac{0.0565}{Z_n}\right)^{\frac{1}{3}} & \left(\frac{5.5943}{Z_n}\right)^{\frac{1}{3}} \end{bmatrix} \tag{15}$$

and letting $\boldsymbol{S}$ be a $m \times n$ matrix of vectors $[L, a, b]^T$, we can rewrite Eq. (8) as follows:

$$\boldsymbol{S} = \boldsymbol{N} \cdot \boldsymbol{A}^* \cdot \boldsymbol{M} \cdot \boldsymbol{P} + \boldsymbol{V}. \tag{16}$$

By using the least square method, the transformation matrix can be derived as

$$\boldsymbol{M} = (\boldsymbol{A}^*)^{-1} \cdot \boldsymbol{N}^{-1} \cdot (\boldsymbol{S} - \boldsymbol{V}) \cdot \boldsymbol{P}^T / (\boldsymbol{P} \cdot \boldsymbol{P}^T). \tag{17}$$

Remark3.1. A^* is derived from the simplification of Eq. (11) to reduce computational complexity. Our future research will seek for a new A^* to make it closer to Eq. (11) and will further improve the integrity of the model under this framework.

3.2. Polynomial terms extension

In Section 3.1, we have established a better transformation from the device RGB space to CIELAB color space. To further improve the transformation accuracy, we propose polynomial terms extension in this section. The root polynomial color correction(RPCC) [19] is taking kth root of each k-order. Instead, our method adds the root polynomial terms to the k-order ordinary polynomial and ensures the order of each root polynomial term is equal to k. The polynomial expansions $\boldsymbol{\rho}_1$, $\boldsymbol{\rho}_2$, $\boldsymbol{\rho}_3$, $\boldsymbol{\rho}_4$ are denoted as follows:

$$
\begin{cases}
\boldsymbol{\rho}_1 = \left(1, r^{\frac{1}{3}}, g^{\frac{1}{3}}, b^{\frac{1}{3}}, \sqrt{r^{\frac{1}{3}}g^{\frac{1}{3}}}, \sqrt{g^{\frac{1}{3}}b^{\frac{1}{3}}}, \sqrt{r^{\frac{1}{3}}b^{\frac{1}{3}}}, \sqrt[3]{r^{\frac{1}{3}}g^{\frac{1}{3}}b^{\frac{1}{3}}}, \sqrt[3]{r^{\frac{1}{3}}g^{\frac{2}{3}}}, \sqrt[3]{r^{\frac{2}{3}}g^{\frac{1}{3}}}, \sqrt[3]{g^{\frac{1}{3}}b^{\frac{2}{3}}}, \sqrt[3]{g^{\frac{2}{3}}b^{\frac{1}{3}}}, \sqrt[3]{r^{\frac{1}{3}}b^{\frac{2}{3}}}, \sqrt[3]{r^{\frac{2}{3}}b^{\frac{1}{3}}}\right)^T \\
\boldsymbol{\rho}_2 = \left(1, r^{\frac{1}{3}}, g^{\frac{1}{3}}, b^{\frac{1}{3}}, \sqrt{r^{\frac{1}{3}}g^{\frac{1}{3}}}, \sqrt{g^{\frac{1}{3}}b^{\frac{1}{3}}}, \sqrt{r^{\frac{1}{3}}b^{\frac{1}{3}}}, \sqrt[3]{r^{\frac{1}{3}}g^{\frac{1}{3}}b^{\frac{1}{3}}}, \sqrt[3]{r^{\frac{1}{3}}g^{\frac{2}{3}}}, \sqrt[3]{r^{\frac{2}{3}}g^{\frac{1}{3}}}, \sqrt[3]{g^{\frac{1}{3}}b^{\frac{2}{3}}}, \sqrt[3]{g^{\frac{2}{3}}b^{\frac{1}{3}}}, \sqrt[3]{r^{\frac{1}{3}}b^{\frac{2}{3}}}, \sqrt[3]{r^{\frac{2}{3}}b^{\frac{1}{3}}},\right. \\
\qquad \left. r^{\frac{2}{3}}, g^{\frac{2}{3}}, b^{\frac{2}{3}}, r^{\frac{1}{3}}g^{\frac{1}{3}}, r^{\frac{1}{3}}b^{\frac{1}{3}}, g^{\frac{1}{3}}b^{\frac{1}{3}}, \sqrt{r^{\frac{2}{3}}g^{\frac{1}{3}}b^{\frac{1}{3}}}, \sqrt{r^{\frac{1}{3}}g^{\frac{2}{3}}b^{\frac{1}{3}}}, \sqrt{r^{\frac{1}{3}}g^{\frac{1}{3}}b^{\frac{2}{3}}}\right)^T \\
\boldsymbol{\rho}_3 = \left(1, r^{\frac{1}{3}}, g^{\frac{1}{3}}, b^{\frac{1}{3}}, \sqrt{r^{\frac{1}{3}}g^{\frac{1}{3}}}, \sqrt{g^{\frac{1}{3}}b^{\frac{1}{3}}}, \sqrt{r^{\frac{1}{3}}b^{\frac{1}{3}}}, \sqrt[3]{r^{\frac{1}{3}}g^{\frac{1}{3}}b^{\frac{1}{3}}}, \sqrt[3]{r^{\frac{1}{3}}g^{\frac{2}{3}}}, \sqrt[3]{r^{\frac{2}{3}}g^{\frac{1}{3}}}, \sqrt[3]{g^{\frac{1}{3}}b^{\frac{2}{3}}}, \sqrt[3]{g^{\frac{2}{3}}b^{\frac{1}{3}}}, \sqrt[3]{r^{\frac{1}{3}}b^{\frac{2}{3}}}, \sqrt[3]{r^{\frac{2}{3}}b^{\frac{1}{3}}},\right. \\
\qquad r^{\frac{2}{3}}, g^{\frac{2}{3}}, b^{\frac{2}{3}}, r^{\frac{1}{3}}g^{\frac{1}{3}}, r^{\frac{1}{3}}b^{\frac{1}{3}}, g^{\frac{1}{3}}b^{\frac{1}{3}}, \sqrt{r^{\frac{2}{3}}g^{\frac{1}{3}}b^{\frac{1}{3}}}, \sqrt{r^{\frac{1}{3}}g^{\frac{2}{3}}b^{\frac{1}{3}}}, \sqrt{r^{\frac{1}{3}}g^{\frac{1}{3}}b^{\frac{2}{3}}}, \\
\qquad r, g, b, r^{\frac{1}{3}}g^{\frac{2}{3}}, r^{\frac{2}{3}}g^{\frac{1}{3}}, g^{\frac{1}{3}}b^{\frac{2}{3}}, g^{\frac{2}{3}}b^{\frac{1}{3}}, r^{\frac{1}{3}}b^{\frac{2}{3}}, r^{\frac{2}{3}}b^{\frac{1}{3}}, r^{\frac{1}{3}}g^{\frac{1}{3}}b^{\frac{1}{3}}, b^{\frac{2}{3}}\sqrt{r^{\frac{1}{3}}g^{\frac{1}{3}}}, r^{\frac{2}{3}}\sqrt{g^{\frac{1}{3}}b^{\frac{1}{3}}}, g^{\frac{2}{3}}\sqrt{r^{\frac{1}{3}}b^{\frac{1}{3}}}, r^{\frac{1}{3}}b^{\frac{1}{3}}\sqrt{r^{\frac{1}{3}}g^{\frac{1}{3}}}, \\
\qquad \left. g^{\frac{1}{3}}b^{\frac{1}{3}}\sqrt{r^{\frac{1}{3}}g^{\frac{1}{3}}}, r^{\frac{1}{3}}g^{\frac{1}{3}}\sqrt{g^{\frac{1}{3}}b^{\frac{1}{3}}}, r^{\frac{1}{3}}b^{\frac{1}{3}}\sqrt{g^{\frac{1}{3}}b^{\frac{1}{3}}}, r^{\frac{1}{3}}g^{\frac{1}{3}}\sqrt{r^{\frac{1}{3}}b^{\frac{1}{3}}}, g^{\frac{1}{3}}b^{\frac{1}{3}}\sqrt{r^{\frac{1}{3}}b^{\frac{1}{3}}}\right)^T \\
\boldsymbol{\rho}_4 = \left(1, r^{\frac{1}{3}}, g^{\frac{1}{3}}, b^{\frac{1}{3}}, \sqrt{r^{\frac{1}{3}}g^{\frac{1}{3}}}, \sqrt{g^{\frac{1}{3}}b^{\frac{1}{3}}}, \sqrt{r^{\frac{1}{3}}b^{\frac{1}{3}}}, \sqrt[3]{r^{\frac{1}{3}}g^{\frac{1}{3}}b^{\frac{1}{3}}}, \sqrt[3]{r^{\frac{1}{3}}g^{\frac{2}{3}}}, \sqrt[3]{r^{\frac{2}{3}}g^{\frac{1}{3}}}, \sqrt[3]{g^{\frac{1}{3}}b^{\frac{2}{3}}}, \sqrt[3]{g^{\frac{2}{3}}b^{\frac{1}{3}}}, \sqrt[3]{r^{\frac{1}{3}}b^{\frac{2}{3}}}, \sqrt[3]{r^{\frac{2}{3}}b^{\frac{1}{3}}},\right. \\
\qquad r^{\frac{2}{3}}, g^{\frac{2}{3}}, b^{\frac{2}{3}}, r^{\frac{1}{3}}g^{\frac{1}{3}}, r^{\frac{1}{3}}b^{\frac{1}{3}}, g^{\frac{1}{3}}b^{\frac{1}{3}}, \sqrt{r^{\frac{2}{3}}g^{\frac{1}{3}}b^{\frac{1}{3}}}, \sqrt{r^{\frac{1}{3}}g^{\frac{2}{3}}b^{\frac{1}{3}}}, \sqrt{r^{\frac{1}{3}}g^{\frac{1}{3}}b^{\frac{2}{3}}}, \\
\qquad r, g, b, r^{\frac{1}{3}}g^{\frac{2}{3}}, r^{\frac{2}{3}}g^{\frac{1}{3}}, g^{\frac{1}{3}}b^{\frac{2}{3}}, g^{\frac{2}{3}}b^{\frac{1}{3}}, r^{\frac{1}{3}}b^{\frac{2}{3}}, r^{\frac{2}{3}}b^{\frac{1}{3}}, r^{\frac{1}{3}}g^{\frac{1}{3}}b^{\frac{1}{3}}, b^{\frac{2}{3}}\sqrt{r^{\frac{1}{3}}g^{\frac{1}{3}}}, r^{\frac{2}{3}}\sqrt{g^{\frac{1}{3}}b^{\frac{1}{3}}}, g^{\frac{2}{3}}\sqrt{r^{\frac{1}{3}}b^{\frac{1}{3}}}, r^{\frac{1}{3}}b^{\frac{1}{3}}\sqrt{r^{\frac{1}{3}}g^{\frac{1}{3}}}, \\
\qquad g^{\frac{1}{3}}b^{\frac{1}{3}}\sqrt{r^{\frac{1}{3}}g^{\frac{1}{3}}}, r^{\frac{1}{3}}g^{\frac{1}{3}}\sqrt{g^{\frac{1}{3}}b^{\frac{1}{3}}}, r^{\frac{1}{3}}b^{\frac{1}{3}}\sqrt{g^{\frac{1}{3}}b^{\frac{1}{3}}}, r^{\frac{1}{3}}g^{\frac{1}{3}}\sqrt{r^{\frac{1}{3}}b^{\frac{1}{3}}}, g^{\frac{1}{3}}b^{\frac{1}{3}}\sqrt{r^{\frac{1}{3}}b^{\frac{1}{3}}}, \\
\qquad \left. r^{\frac{4}{3}}, g^{\frac{4}{3}}, b^{\frac{4}{3}}, rg^{\frac{1}{3}}, rb^{\frac{1}{3}}, gr^{\frac{1}{3}}, gb^{\frac{1}{3}}, br^{\frac{1}{3}}, bg^{\frac{1}{3}}, r^{\frac{2}{3}}g^{\frac{2}{3}}, g^{\frac{2}{3}}b^{\frac{2}{3}}, r^{\frac{2}{3}}b^{\frac{2}{3}}, r^{\frac{2}{3}}g^{\frac{1}{3}}b^{\frac{1}{3}}, g^{\frac{2}{3}}r^{\frac{1}{3}}b^{\frac{1}{3}}, b^{\frac{2}{3}}r^{\frac{1}{3}}g^{\frac{1}{3}}\right)
\end{cases}
\tag{18}
$$

We increase the dimension of the base vector to improve the accuracy of the polynomial regression. Hong et al. [12, 13] pointed out that the regression accuracy in fact relys on the specific polynomial terms. Based on their research, only the 3-component cross term of $r^{\frac{1}{3}}$, $g^{\frac{1}{3}}$, $b^{\frac{1}{3}}$ are used for the polynomial expansions of quadratic and cubic polynomial. It is worth pointing out that the reduction of both the average ΔE and maximum ΔE is significantly subject to the three-dimensional cross term of $r^{\frac{1}{3}}$, $g^{\frac{1}{3}}$, $b^{\frac{1}{3}}$. For higher order polynomials, only the ordinary items are considered rather than root items because of the oscillating appearance. Compared with the methods mentioned in Section 2.3, our method increases the number of

polynomial terms to improve the accuracy of color characterization. But for each $\rho_i (i = 1, 2, 3, 4)$, the highest degree of polynomial basis is $\frac{i}{3}$. The comparative tests will be performed in Section 4, which are based on such a standard selected basis. Although the number of base terms is different for these methods(mentioned in Section 2.3), this standard ensures that the comparison is reasonable and significant.

4. Experiment

To verify the performance of our method, we test our method with the public data and carry out camera experiments. For each set of data, we compare the results with other methods mentioned in Section 2.3. The parameters for evaluating the performance of the method are include the mean ΔE_{ab} color difference (Section 2.2) for all color samples $\overline{\Delta E}$, the maximum ΔE_{ab} color difference ΔE_{max}, the mean error of each color attribute $\overline{\Delta L}$, $\overline{\Delta a}$, $\overline{\Delta b}$, the maximum error of each color attribute ΔL_{max}, Δa_{max}, Δb_{max}. In addition, ΔE, the error and the corrected error are all referring to the color difference in CIELAB color space without specification in this paper.

4.1. Tests with public data

We test our method using the numerical data given in the appendix of the literature[14] proposed by Hardeberg. The data is obtained from the AGFA Arcus II scanner with the AGFA IT8.7/2 color chart. Besides the characterization methods listed in the literature, we compare our method with the others. The results are shown in Table 1.

Table 1 shows that our method obtains good results for each order polynomial, especially for the low-order-polynomial. When the first order polynomial of our method is used, the average ΔE is 1.013, which is much better compared by using Hardeberg's method. Meanwhile, both the average ΔE and the max ΔE have come close to the optimal results (i.e., the results of the third order polynomial) of Hardeberg's method. When the second order polynomial of our method is used, the average ΔE and the max ΔE have already outperformed the optimal results of Hardeberg's method. As for the third order polynomial, the max ΔE of our method is 3.213, which closes to the very good quality based on the color difference evaluation criterion introduced in Section 2.2. As we pointed the description in **Remark3.1**, our method would deteriorate to Hardeberg's method if we use the classic polynomial expansion $\boldsymbol{\rho}_k$ mentioned in Section 2.1. However, we add root polynomial cross-terms to each order of the model and the added cross-terms are different from the ordinary polynomial cross-terms in that they are smoother around the achromatic region. From the test results, it can obviously improve the accuracy of color characterization.

As for RPCC method, it is unfair to be compared here as the number of polynomial terms is significantly different. From $\rho 1$ to $\rho 4$, RPCC has 3, 6, 13 and 22 terms and our method has 14, 23, 42 and 57 terms, but that is because the purpose between RPCC and our method is different. RPCC focuses on achieving

Table 1: Test results with public data.

Model type	$\overline{\Delta E}$	ΔE_{max}	$\overline{\Delta L}$	ΔL_{max}	$\overline{\Delta a}$	Δa_{max}	$\overline{\Delta b}$	Δb_{max}
RGB–CIEXYZ[12],ρ1	4.841	22.939	1.276	3.715	2.782	20.932	3.135	15.354
RGB–CIELAB[20],ρ1	22.270	49.111	15.310	34.052	8.422	37.251	9.056	40.062
Hardeberg[14],ρ1	5.652	23.961	3.241	11.345	2.234	23.304	2.987	12.645
RPCC[19],ρ1	4.591	30.912	0.873	7.089	3.057	26.331	2.640	15.491
Our method,ρ1	**1.013**	**4.782**	**0.342**	**2.547**	**0.569**	**3.313**	**0.591**	**3.389**
RGB–CIEXYZ[12],ρ2	2.989	28.246	0.458	3.585	1.653	21.718	1.956	28.089
RGB–CIELAB[20],ρ2	8.858	40.349	2.854	14.054	5.077	25.858	5.024	29.930
Hardeberg[14],ρ2	1.496	12.448	0.348	2.352	1.166	12.348	0.579	3.311
RPCC[19],ρ2	4.530	22.746	0.707	2.743	2.830	20.962	2.899	13.362
Our method,ρ2	**0.816**	**3.849**	**0.284**	**2.034**	**0.464**	**2.862**	**0.458**	**2.718**
RGB–CIEXYZ[12],ρ3	2.170	20.903	0.427	2.490	1.306	18.576	1.348	13.276
RGB–CIELAB[20],ρ3	5.386	30.792	1.385	9.775	3.207	23.060	3.114	19.784
Hardeberg[14],ρ3	0.918	4.666	0.289	2.069	0.621	4.588	0.427	2.792
RPCC[19],ρ3	4.514	21.058	0.714	3.066	2.824	20.587	2.957	16.292
Our method,ρ3	**0.629**	**3.213**	**0.251**	**1.746**	**0.326**	**2.418**	**0.363**	**2.341**
RGB–CIEXYZ[12],ρ4	1.537	14.269	0.301	2.716	0.912	12.222	0.95	11.197
RGB–CIELAB[20],ρ4	3.565	20.605	0.835	7.765	2.238	17.501	1.984	10.34
Hardeberg[14],ρ4	0.7	2.863	0.27	1.883	0.391	2.58	0.375	1.72
RPCC[19],ρ4	4.04	23.161	0.641	2.919	2.529	22.207	2.587	18.576
Our method,ρ4	**0.514**	**2.861**	**0.232**	**1.599**	**0.268**	**2.304**	**0.268**	**1.508**

exposure invariance, but our method aims to improve the accuracy of color characterization under the same exposure condition. On one hand, our color backward deduction model converts color signal from digital RGB to CIELAB space instead of CIEXYZ space (since the Euclidean distance in CIELAB space corresponds quite well to perceptual color differences), which can reduce the visual error of color characterization. On the other hand, based on RPCC method, high order extension of the polynomial root terms is proposed to further improve the conversion accuracy. Meanwhile, the performance of our method with low-order polynomial is comparable to that of other methods with high-order polynomial, which could help to reduce the influence of Runge effect. Although our method increases the number of polynomial terms, the highest degree of polynomial basis is $\frac{i}{3}$ for each $\rho_i (i = 1, 2, 3, 4)$, our method is an extension of RPCC method.

Then, we present the error analysis of our method in Fig. 3 with the numerical data given in the literature [14]. The subgraph above is a scatter diagram which describes the corrected error of three channels for each patch in the public data. It is not difficult to find that the error of the red channel is relatively stable for the transformation. The error of the blue channel is much unstable compared with other channels. The following two subgraphs show the expectation and the variance of the corrected errors of the three channels for all patches. We can find that the green channel is sensitive for transformation. The expected absolute value of the blue channel error is much higher.

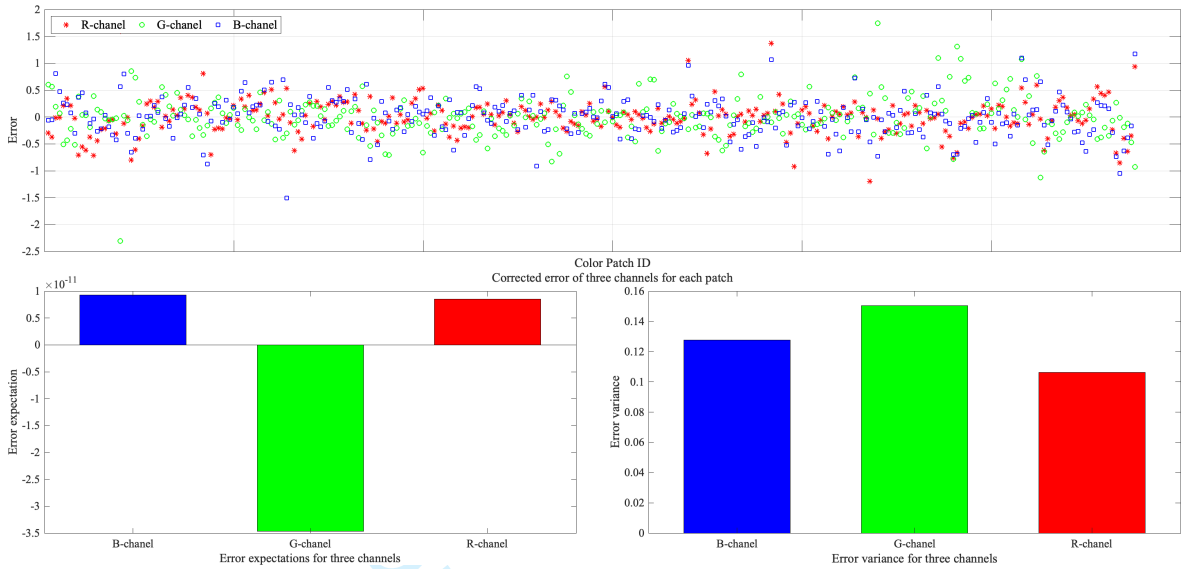

Figure 3: Error analysis of three channels with public data.

To verify whether our model is overfitting, we decrease the number of training data($N_{training}$) used for regression. The other data($N_{testing} = N - N_{training}$, $N = 288$) are used for testing. With our proposed method(from the first order to the fourth order polynomial), the corrected error on the training set and testing set are shown in Fig. 4 and 5, respectively. As can be seen from the figures, when the number of training data is less than the number of parameters, the results are unstable. As the number of training data is increasing, the error converges to a constant value(from the first order to the fourth order polynomial) and the results become stable.

Furthermore, we compare the corrected error($\rho 4$) with other methods($\rho 4$) based on the testing data set. Since RPCC method focuses on the invariance of exposure(it is unfair to compare), we compare our method with other three methods except RPCC. The results are shown in Table 2. It can be seen that even if the number of the training data is reduced to 108, the mean error of our method on the testing set only increases by 0.476 ΔE units. When the number of training data is larger than the number of parameters, the results of our method are obviously better than other three methods. Although the results get unusable with little sample, it is not a problem in practice since as much as possible data should be used for training to produce high quality results.

In the above experiments, the corrected errors are compared all in CIELAB color space. Since the classical methods convert the digital RGB to CIEXYZ color space, we also compare the corrected error of all the data(given in the literature[14], $N = 288$) in CIEXYZ color space with the classical methods. The comparison results are shown in Table 3. We also can see that even in CIEXYZ color space, the corrected error of our method is lower than that of the classical methods. The optimal result is obtained with the fourth order polynomial of our method.

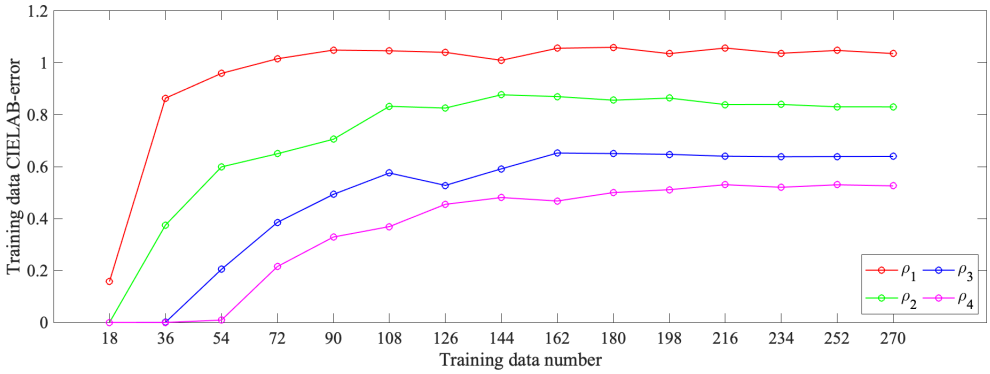

Figure 4: Corrected CIELAB error on the training set with public data.

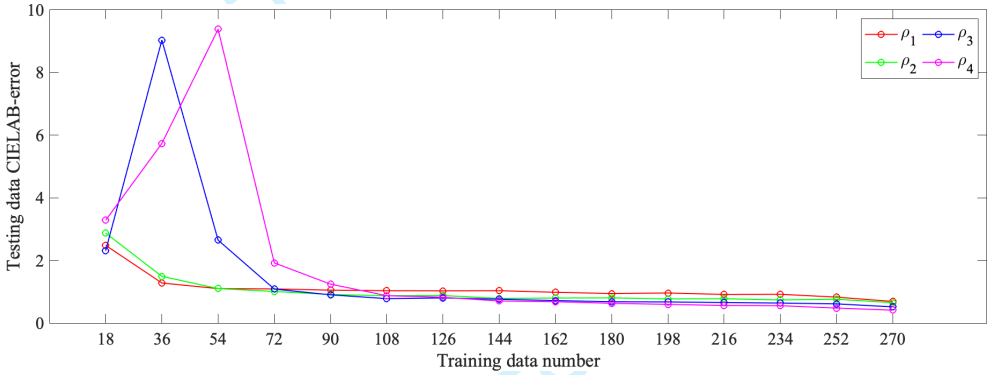

Figure 5: Corrected CIELAB error on the testing set with public data.

Table 2: Corrected error on the testing set using the fourth order polynomial.

Patches		Testing $\overline{\Delta E}$			
N_{traing}	$N_{testing}$	RGB–CIEXYZ[12],$\boldsymbol{\rho}$4	RGB–CIELAB[20],$\boldsymbol{\rho}$4	Hardeberg[14],$\boldsymbol{\rho}$4	Our method,$\boldsymbol{\rho}$4
270	18	0.979	4.026	0.552	**0.435**
252	36	1.041	3.494	0.719	**0.517**
234	54	1.056	3.412	0.653	**0.514**
216	72	1.768	4.105	0.766	**0.616**
198	90	1.825	4.165	0.791	**0.638**
180	108	1.591	4.152	0.769	**0.646**
162	126	1.598	4.872	0.763	**0.701**
144	144	1.533	4.242	0.823	**0.754**
126	162	1.864	4.765	0.975	**0.822**
108	180	1.612	4.298	0.846	**0.911**
90	198	1.913	4.877	0.890	**1.155**
72	216	2.065	6.938	1.098	**2.810**
54	234	2.303	7.490	1.538	**12.561**
36	252	9.932	62.825	4.916	**6.328**

Table 3: Corrected error of all data in CIEXYZ color space.

Model type	$\overline{CIEXYZ\_error}$
RGB–CIEXYZ[12],$\boldsymbol{\rho}$1	1.141
RGB–CIELAB[20],$\boldsymbol{\rho}$1	10.045
Our method,$\boldsymbol{\rho}$ 1	**0.559**
RGB–CIEXYZ[12],$\boldsymbol{\rho}$2	0.721
RGB–CIELAB[20],$\boldsymbol{\rho}$2	4.199
Our method,$\boldsymbol{\rho}$ 2	**0.459**
RGB–CIEXYZ[12],$\boldsymbol{\rho}$3	0.511
RGB–CIELAB[20],$\boldsymbol{\rho}$3	2.081
Our method,$\boldsymbol{\rho}$ 3	**0.386**
RGB–CIEXYZ[12],$\boldsymbol{\rho}$4	0.396
RGB–CIELAB[20],$\boldsymbol{\rho}$4	1.199
Our method,$\boldsymbol{\rho}$ 4	**0.332**

The error analysis in CIEXYZ color space is similar to the overfitting experiment in CIELAB color space. We also gradually reduce the number of color patches used for training samples in the color checker, and the rest are test samples. The CIEXYZ error with our method based on the training set and testing set are shown in Fig. 6 and 7, respectively. It can be seen that the CIEXYZ error trend of our method is similar to the CIELAB error trend above. The results are also stable and convergent.

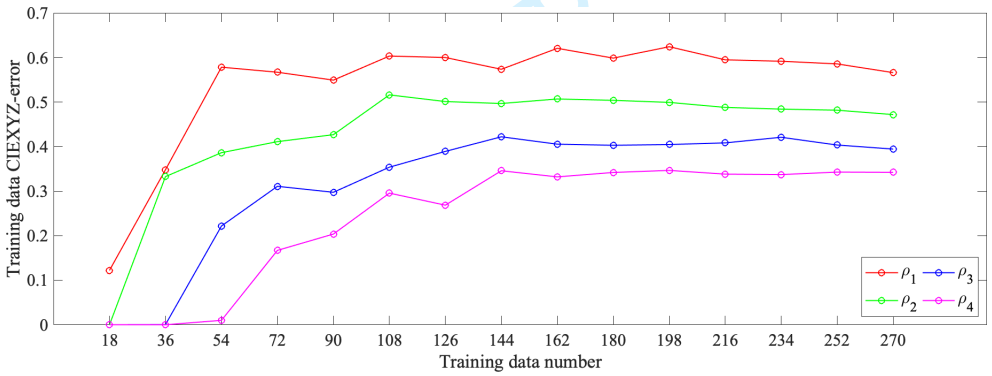

Figure 6: Corrected CIEXYZ error on the training set with public data.

In summary, based on the idea of RPCC method, our method expand terms to the basis of polynomial. Although the number of polynomial terms is increased, the result of color characterization is greatly improved and the computational complexity is not increased obviously. In addition, the first order polynomial results of our method are similar to the higher order polynomial results of other methods(e.g. the results of Hardeberg's method(ρ3, 20 terms) are similar to the results of our method(ρ1, 14 terms)), which means that our method could be helpful to reduce the influence of Runge effect and achieve exposure invariance with high conversion accuracy.

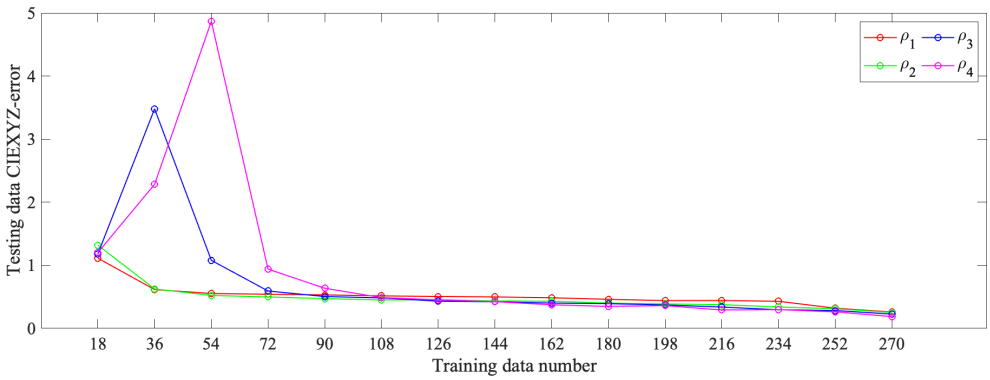

Figure 7: Corrected CIEXYZ error on the testing set with public data.

4.2. Experiment with actual light source

We perform camera characterization under actual light source with the experimental set-up as shown in Fig. 8. Two line illuminants project light on the surface of the object. The illuminants should be carefully set up in order to preserve the uniformity of light energy, which is crucial to the color characterization. A line scan camera is placed in the normal direction to the object surface while the lighting direction is projected at the angle of 45.

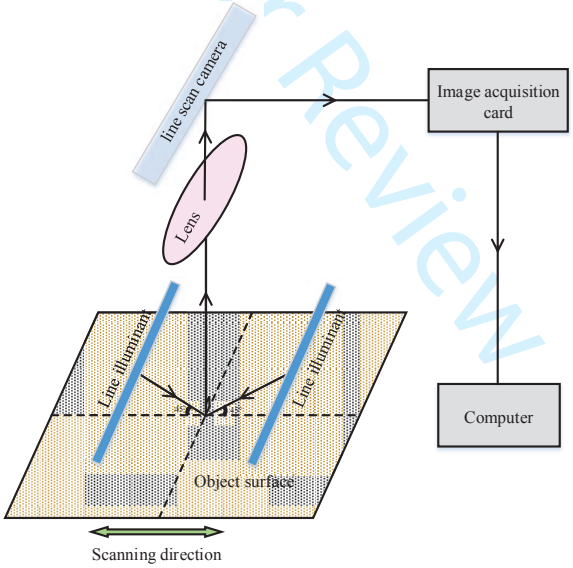

Figure 8: Schematic diagram of actual light source experimental set-up.

When the equipment starts to work, the reflected light passes through the lens into the line scan camera, which can perform optical-electrical conversion. At last, the image acquisition card captures the images and the computer saves the images. This equipment adopts line scan camera, which can capture only a line of the image at each time. Therefore, the imaging system is required to move along the main scanning

direction until the collection of a frame image is finished.

The exposure should be set to prevent color clipping. Meanwhile, the aperture size and exposure time is fixed during the experiment. A X-Rite IT8.7/2 color chart on Kodak Ektacolour material is used. The color checker covers a large color gamut in CIELAB color space, whose nominal CIELAB values are specied by the manufacture. The raw images of the color checker are captured and the patches images are manually divided. Then we calculate the average responses of 90% of pixies in each patch, except for the marginalized pixies, as the output values of the camera RGB. The dark current is excluded from the average RGB responses. Next, the linearization of the camera RGB values is carried out to obtain RGB values proportional to the intensity of the input light. In addition, as the light source for this study is cultural relics-friendly linear array LED, the intensity distribution of this illuminant deceases generally from the middle to both sides, which results in high grey value in the middle of the captured image and low grey value in both sides. Therefore, a standard white board is used to correct the uniformity and repeatability of the captured image's brightness. At last, the linearized and homogenized camera RGB values and CIELABs are utilized to build the color characterization model described in Section 3. We test the model using the leave-one-out method. Specifically, the model is built based on all patches except one of the color checker. Then we test the model on the rest of the patches. The process is repeated for all patches and the mean ΔE in CIELAB color space is calculated. The results can be seen in Table 4.

Table 4: Experiment results with actual light source.

Model type	$\overline{\Delta E}$	ΔE_{max}	$\overline{\Delta L}$	ΔL_{max}	$\overline{\Delta a}$	Δa_{max}	$\overline{\Delta b}$	Δb_{max}
RGB–CIEXYZ[12],$\boldsymbol{\rho}$1	4.419	41.653	1.057	11.682	2.595	16.928	2.655	41.595
RGB–CIELAB[20],$\boldsymbol{\rho}$1	13.955	43.347	5.672	23.717	7.259	27.000	7.936	33.710
Hardeberg[14],$\boldsymbol{\rho}$1	5.379	48.766	1.351	12.460	3.235	47.764	3.173	27.281
RPCC[19],$\boldsymbol{\rho}$1	4.419	41.653	1.057	11.682	2.595	16.927	2.655	41.595
Our method,$\boldsymbol{\rho}$1	**3.803**	**22.216**	**1.107**	**11.249**	**1.998**	**10.280**	**2.404**	**20.929**
RGB–CIEXYZ[12],$\boldsymbol{\rho}$2	3.982	38.010	0.921	9.147	2.152	11.323	2.575	37.988
RGB–CIELAB[20],$\boldsymbol{\rho}$2	7.366	23.650	2.577	17.009	3.801	18.563	4.497	21.125
Hardeberg[14],$\boldsymbol{\rho}$2	4.262	21.941	0.986	10.436	2.334	21.502	2.774	20.131
RPCC[19],$\boldsymbol{\rho}$2	4.438	37.732	1.251	14.177	2.362	11.724	2.774	37.178
Our method,$\boldsymbol{\rho}$2	**3.395**	**15.253**	**0.897**	**9.845**	**1.822**	**9.933**	**2.200**	**12.368**
RGB–CIEXYZ[12],$\boldsymbol{\rho}$3	3.967	45.824	0.906	8.110	2.158	45.757	2.543	27.774
RGB–CIELAB[20],$\boldsymbol{\rho}$3	4.858	16.812	1.393	13.148	2.658	13.459	3.031	15.231
Hardeberg[14],$\boldsymbol{\rho}$3	3.555	13.064	0.884	9.904	1.845	10.688	2.348	10.876
RPCC[19],$\boldsymbol{\rho}$3	4.238	34.136	1.201	13.425	2.138	10.574	2.782	32.665
Our method,$\boldsymbol{\rho}$3	**3.029**	**13.459**	**0.815**	**9.781**	**1.679**	**9.673**	**1.906**	**11.826**
RGB–CIEXYZ[12],$\boldsymbol{\rho}$4	3.696	34.889	0.853	8.480	1.960	12.412	2.489	34.514
RGB–CIELAB[20],$\boldsymbol{\rho}$4	3.758	14.323	0.953	11.589	2.132	11.008	2.288	11.238
Hardeberg[14],$\boldsymbol{\rho}$4	3.177	13.318	0.817	9.698	1.723	9.643	2.036	10.807
RPCC[19],$\boldsymbol{\rho}$4	4.054	40.682	1.083	12.673	2.143	11.070	2.634	39.472
Our method,$\boldsymbol{\rho}$4	**2.892**	**13.461**	**0.754**	**9.745**	**1.611**	**8.612**	**1.806**	**11.092**

From the table we can see that our method performs better than other four methods and gives good results, that is, the mean ΔE is below three units when the fourth order polynomial is used. When comparing the results with the color difference rules mentioned in Section 2.2, the average error is hardly perceptible and the maximal error is acceptable.

The color difference comparisons between our method and each other method for each color patch are shown in Fig. 9-12. It can be seen that the color corrected error of each patch in our method is significantly lower than that in other four methods. For some patches, such as the patches with low lightness, they have a relatively high color error due to low signal-to-noise ratio of the camera, but our method is still superior to other four methods.

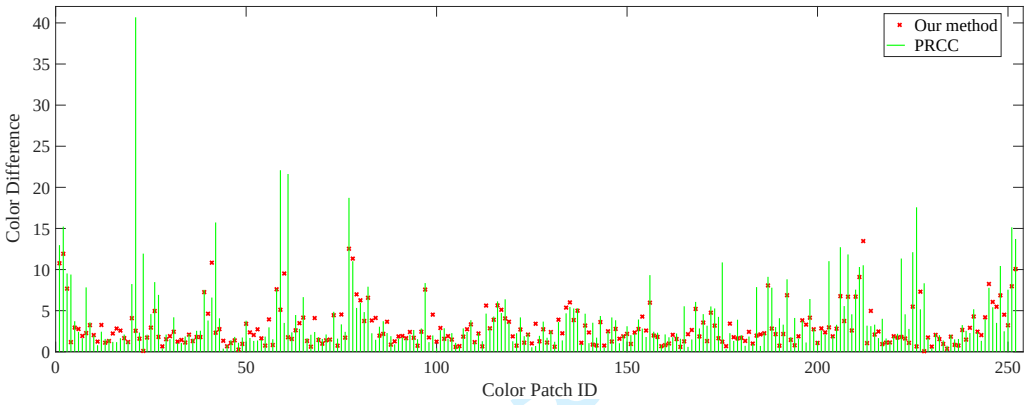

Figure 9: Color difference comparison between our method and RPCC using fourth order polynomial ($\rho 4$).

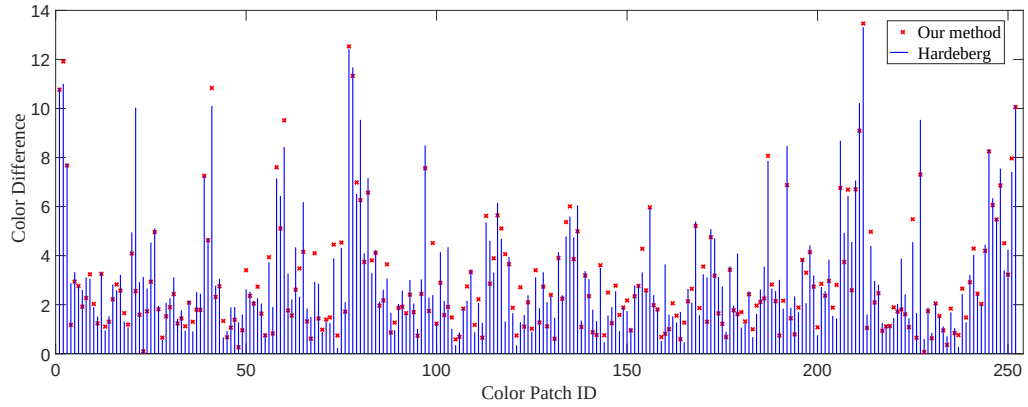

Figure 10: Color difference comparison between our method and Hardeberg's method using fourth order polynomial ($\rho 4$).

Furthermore, in order to analyze the relationship between color corrected errors and color attributes, ΔE vs. L, ΔE vs. a and ΔE vs. b of our method and RPCC method with the fourth order polynomial are shown respectively in Fig. 13-15. In Fig. 13, we can see that color samples with high brightness are more

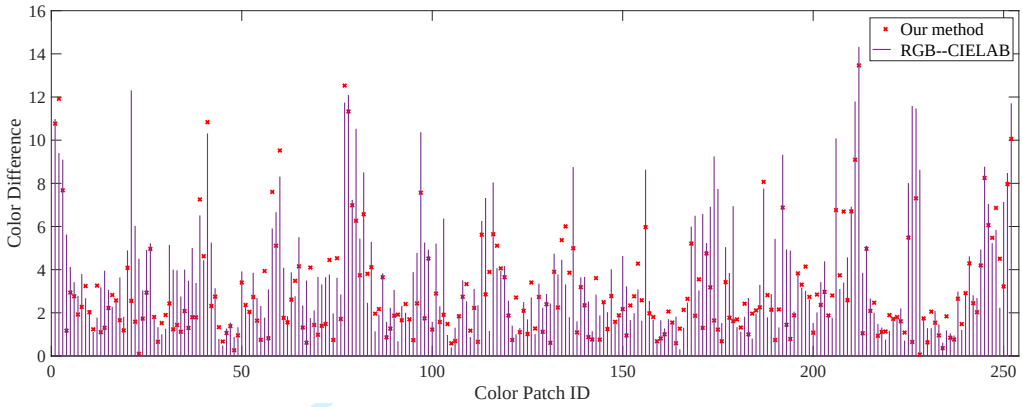

Figure 11: Color difference comparison between our method and RGB–CIELAB using fourth order polynomial ($\rho 4$).

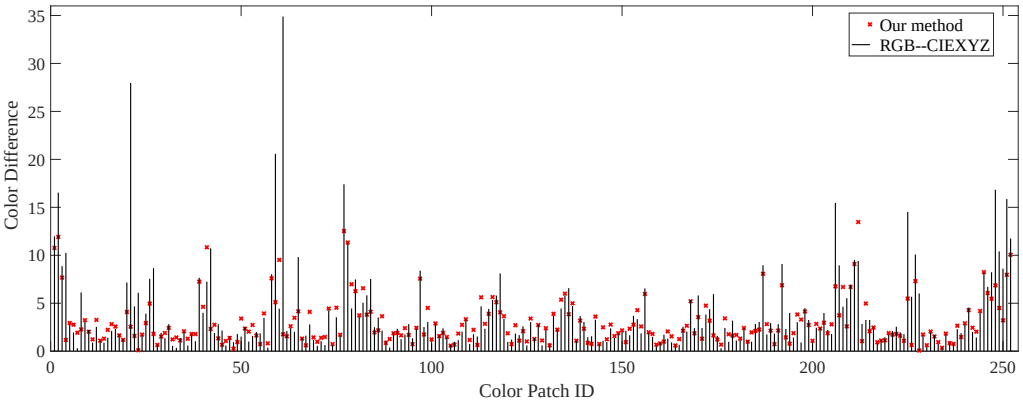

Figure 12: Color difference comparison between our method and RGB–CIEXYZ using fourth order polynomial ($\rho 4$).

accurate than the ones with low brightness. In Fig. 14 and Fig. 15, the neutral colors have lower corrected accuracy. Dark neutral colors have the maximal color corrected errors. The results in Fig. 13-15 suggest that our method has advantages in color characterization with lower brightness and neutral colors.

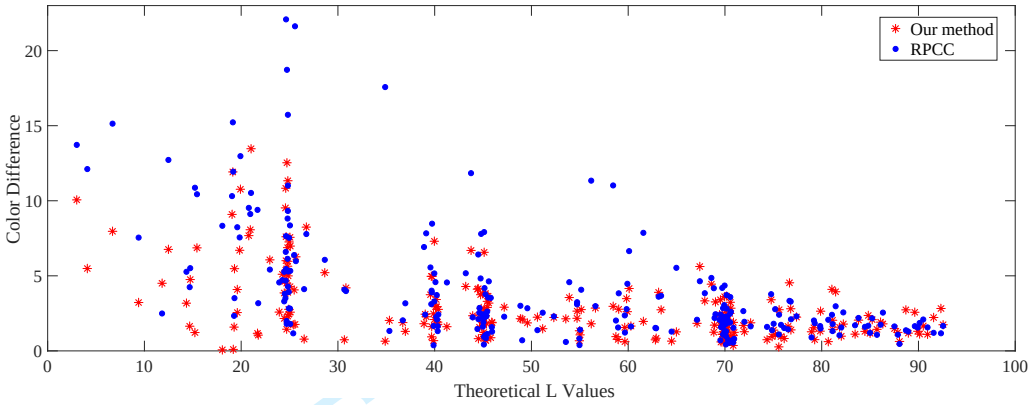

Figure 13: The plot of the relation between color corrected error and L color component using fourth order polynomial ($\rho 4$).

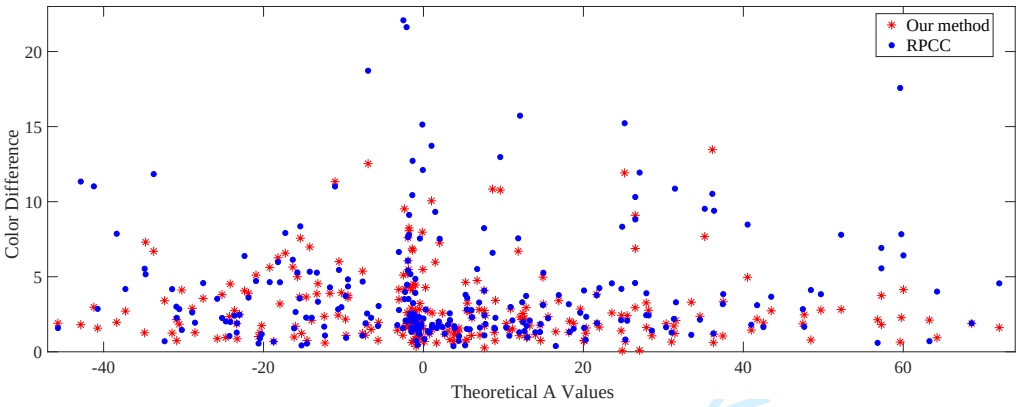

Figure 14: The plot of the relation between color corrected error and A color component using fourth order polynomial ($\rho 4$).

In order to illustrate whether the color characterization model can be normalized in practical application, we divid the color patches of the X-Rite IT8.7/2 color chart as described in Section 4.1(systematically reduce the number of training samples, and the rest are test samples). The results with our method under the actual light source are reported in Fig. 16 and 17. From the figures, the errors of the color characterization model are still convergent and stable in practice.

Furthermore, we use a new chart(Macbeth ColorChecker) as the test sample and the X-Rite IT8.7/2 color chart as the training sample for the test. The errors of the test sample are shown in Table 5. Since RPCC method focuses on exposure invariance(it is unfair to compare), we compare with the other three methods. As can be seen from the results, our method work well.

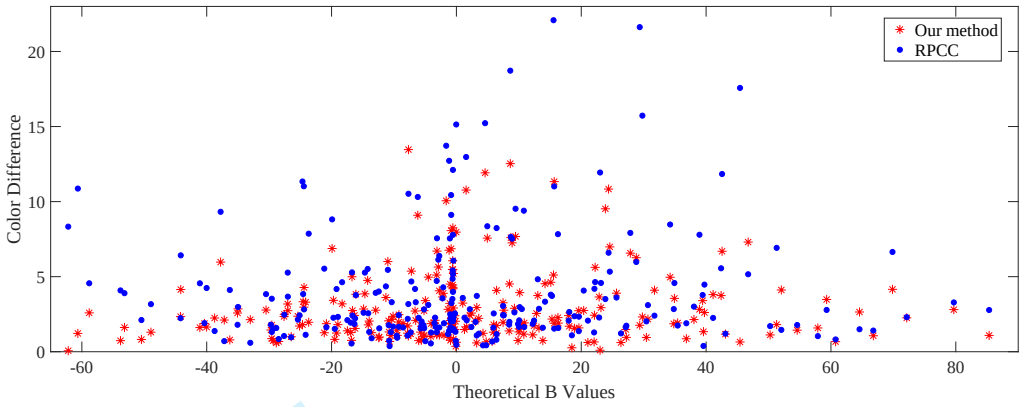

Figure 15: The plot of the relation between color corrected error and B color component using fourth order polynomial ($\rho 4$).

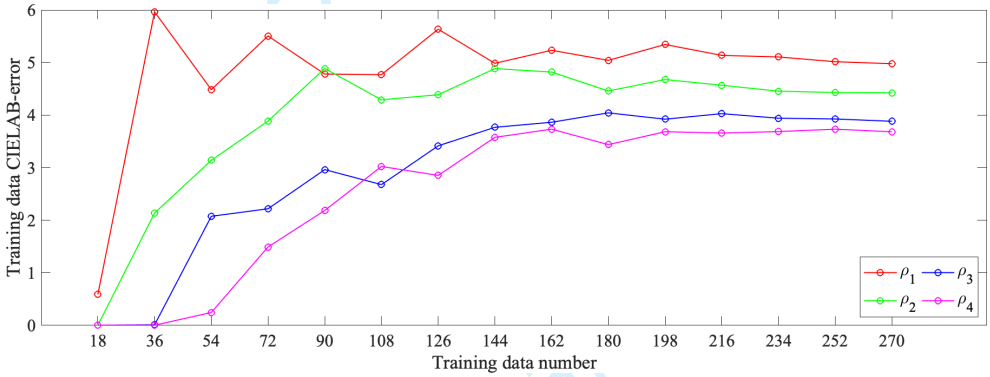

Figure 16: Corrected CIELAB error on the training set with actual light source.

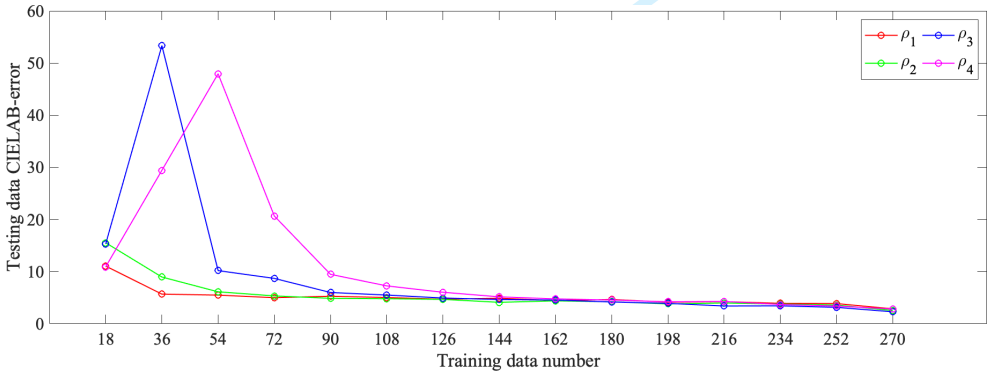

Figure 17: Corrected CIELAB error on the testing set with actual light source.

Table 5: Corrected error of Macbeth ColorChecker.

Model type	RGB–CIEXYZ[12],$\boldsymbol{\rho}$4	RGB–CIELAB[20],$\boldsymbol{\rho}$4	Hardeberg[14],$\boldsymbol{\rho}$4	Our method,$\boldsymbol{\rho}$4
$\overline{\Delta E}$	4.115	4.923	3.501	3.073

Finally, to illustrate the noise influence on the color characterization model, we add 1%, 5% and 10% gaussian noise to the X-Rite IT8.7/2 color chart and then compute the three noise color charts for color correction. The results are shown in the Table 6. It can be seen that the noise leads the corrected error to be higher, but the errors can be controlled. The results become better as the degree of the polynomial increases. Compared with the color difference evaluation standard proposed in Section 2.2, the color correction effect is acceptable even with 10% gaussian noise.

Table 6: Corrected error of noise color checkers.

Model type	No noise,$\overline{\Delta E}$	1 % noise,$\overline{\Delta E}$	5% noise,$\overline{\Delta E}$	10% noise,$\overline{\Delta E}$
Our method,$\boldsymbol{\rho}$ 1	3.803	4.384	4.692	6.182
Our method,$\boldsymbol{\rho}$ 2	3.395	3.919	4.274	5.541
Our method,$\boldsymbol{\rho}$ 3	3.029	3.456	3.738	5.029
Our method,$\boldsymbol{\rho}$ 4	2.892	3.276	3.668	4.819

5. Conclusions

In this paper, we propose a complete transformation model form digital RGB responses to CIELAB colorimetric values considering the interrelations among the standard CIE color spaces. Moreover, the polynomial root terms extension is constructed to further improve the transformation accuracy. The test data given in the literature are used to compare the proposed method and the previous methods. Besides, camera experiments are carried out to verify the performance of our method. The results show that the method presented in this paper outperforms its predecessors in color characterization accuracy. Our method borrows from the idea of RPCC method, but it is different from RPCC. The main purpose is to improve the accuracy of color characterization under the same exposure condition. Moreover, the computational complexity does not increase significantly, so the proposed method is an extension of RPCC method. In addition, it should be note that some researchers used camera's RGB responses or tristimulus values for recovering the spectral information from the colorimetric information[22, 23, 24]. With the method proposed in this paper, colorimetric error can be reduced significantly, therefore, the spectral reproduction results can be futher improved.

Acknowledgments

This work is supported by National Natural Science Foundation of China(No.11601416), the China Postdoctoral Science Foundation (No.2018M640968) and the Fundamental Research Funds for the Central Universities (No.XTR042019005)

References

[1] Molada-Tebar A, Lerma J L, Marqués-Mateu. Camera characterization for improving color archaeological documentation. Color Res. Appl. 2017;43(14):47-57.

[2] Barni M, Pelagotti A, Piva A. Image processing for the analysis and conservation of paintings: opportunities and challenges. Signal Processing Magazine IEEE. 2005;22(5):141-144.

[3] Parry R. Digital heritage and the rise of theory in museum computing. Museum Management and Curatorship. 2005;20(4):333-348.

[4] Sharma G, Bala R. Digital Color Imaging Handbook. Boca Raton, FL, USA: CRC Press; 2010.

[5] Hung PC. Colorimetric calibration for scanners and media. Proc SPIE. 1991;1448:164-174.

[6] Hung PC. Colorimetric calibration in electronic imaging devices using a look-up table model and interpolations. Electronic Imag. 1993;2:53-61.

[7] Kang HR. Colour scanner calibration. Imaging Sci Tech. 1992;36:162-170.

[8] Kang HR, Anderson PG. Neural network applications to the colour scanner and printer calibrations. Electronic Imag. 1992;1:125-134.

[9] Johnson T. Methods for characterizing colour scanners and digital cameras. Displays. 1996;16(4):183-191.

[10] Mou TS, Shen HL. Colorimetric characterization of imaging device by total color difference minimization. Journal of Zhejiang University Science A: Applied Physics & Engineering. 2006;7(6):1041-1045.

[11] Kang HR, Anderson PG. Neural network applications to the color scanner and printer calibrations. Journal of Electronic Imaging. 1992;1(1):125-135.

[12] Hong G, Luo MṘ, Rhodes PA.. A study of digital camera colorimetric characterization based on polynomial modeling. Color Res. Appl. 2001;26(1):76-84.

[13] Hong G, Han B, Luo M.R. Colorimetric characterisation of low-end digital camera and its application for on-screen texture visualisation. In: International Conference on Image Processing. IEEE;2000.

[14] Hardeberg JY. Acquisition and Reproduction of Colour Images:Colorimetric and Multispectral Approaches. Universal Publishers dissertation.com, Parkland. FL2001.

[15] Hardeberg JY, Schmitt F, Tastl I, Brettel H, Crettez JP. Color management for color facsimile. In Proc. IS&T and SIDs 4th Color Imaging Conf.: Color Science, Systems and Applications, Scottsdale;1996. p 108C113.

[16] Andersen CF, Hardeberg JY. Colorimetric Characterization of Digital Cameras Preserving Hue Planes. In: Proc. 13th Color Imag. Conf. (CIC);2005:141-146.

[17] Huang X, Yu H, Shi J, Tai Y. Improvement on the polynomial modeling of digital camera colorimetric characterization. Optoelectronic Imaging and Multimedia Technology III. International Society for Optics and Photonics;2014.

[18] Finlayson GD, Drew M. Constrained least-squares regression in color spaces. Electron Imaging. 1997;4:484-493.

[19] Finlayson GD, Mackiewicz M, Hurlbert A. Color Correction Using Root-Polynomial Regression. IEEE Transactions on Image Processing. 2015;24(5):1460-1470.

[20] Sun B, Liu H, Zhou S, Li W. Evaluating the performance of polynomial regression method with different parameters during color characterization. Mathematical Problems in Engineering. 2014.

[21] Abrardo A, Cappellini V, Cappellini M, Mecocci A. Art-works colour calibration using the VASARI scanner. In Proceedings of IS&T and SID's 4th Color Imaging Conference. Color Science, Systems and Applications; 1996:94C97.

[22] Zhang X, Wang Q, Li J, Zhou X, Yang Y, Xu H. Estimating spectral reflectance from camera responses based on CIE XYZ tristimulus values under multiilluminants. Color Res. Appl. 2017;42(1):68-77.

[23] Cao B, Liao N, Cheng H. Spectral reflectance reconstruction from RGB images based on weighting smaller color difference group. Color Res. Appl. 2017;42(3):327-332.

[24] Amiri MM, Fairchild MD. A strategy toward spectral and colorimetric color reproduction using ordinary digital cameras. Color Res. Appl. 2018;43:675-684.

Author Biographies

Jing Ji received the B.S. degree in Computer Science and Technology and M.S. degree in Computer Application Technology from Chang'an University, Xi'an, China, in 2005 and 2008 respectively. she is currently working towards the Ph.D. degree at the School of Mechanical Engineering, Xi'an Jiaotong University. Her research interests reside in colorimetry and digital image processing.

Suping Fang received his B.S. and M.S. degrees from Xi'an Jiaotong University in 1983 and 1986, respectively. He received his Ph.D. in precision engineering from Kyoto University, Japan, in 1996. From 1996 to 2004, he also worked successively at Kyoto University, Ritsumeikan University in Japan. Currently, he is a professor at Xi'an Jiaotong University. His research interests mainly focused on high fidelity digitization of cultural heritage involving colorimetry, digital image processing and optical electromechanical integration technology.

Zhengyuan Shi received the B.S. degree from the Department of Mathematics, Nanjing Agricultural University, China in 2018. Now he is a Master student in Xi'an Jiaotong University. His research interests include computational fluid dynamics, image processing, and scientific computing.

Qing Xia received the B.S. degree from the Department of Mathematics, Xi'an Jiaotong University, China in 2019. Now he is a Master student in Xi'an Jiaotong University. His research interests include Additive Manufacturing (3D Printing), image processing, and scientific computing.

Yibao Li received the M.S. and Ph.D. degrees in Applied Mathematics from Korea University, Korea, in 2011 and 2013, respectively. Before he joined the School of Mathematics and Statistics, Xi'an Jiaotong University, China in 2014, he held a research position in Department of Computational Science and Engineering, Yonsei University, Korea. He is currently an associate professor at the Department of Applied Mathematics. His research interests include image processing, computational fluid dynamics, and scientific computing.

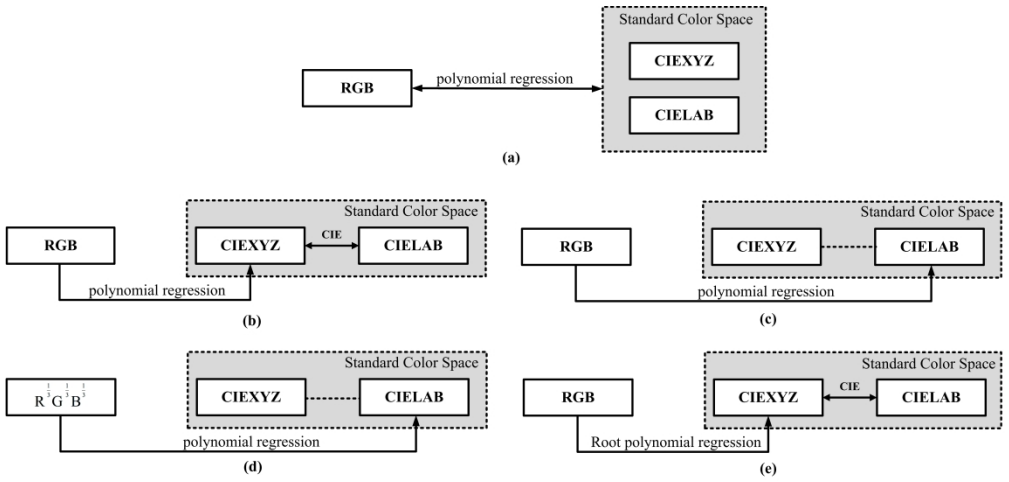

552x262mm (600 x 600 DPI)

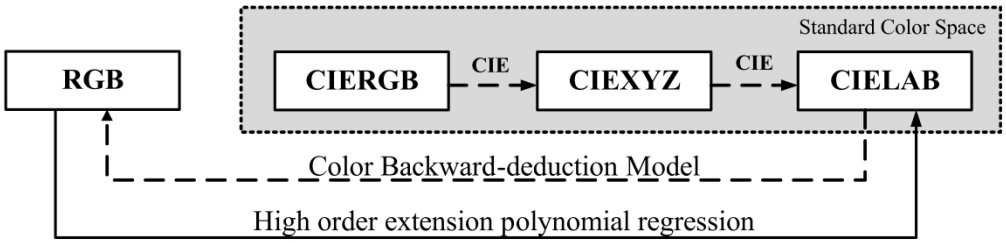

296x73mm (600 x 600 DPI)

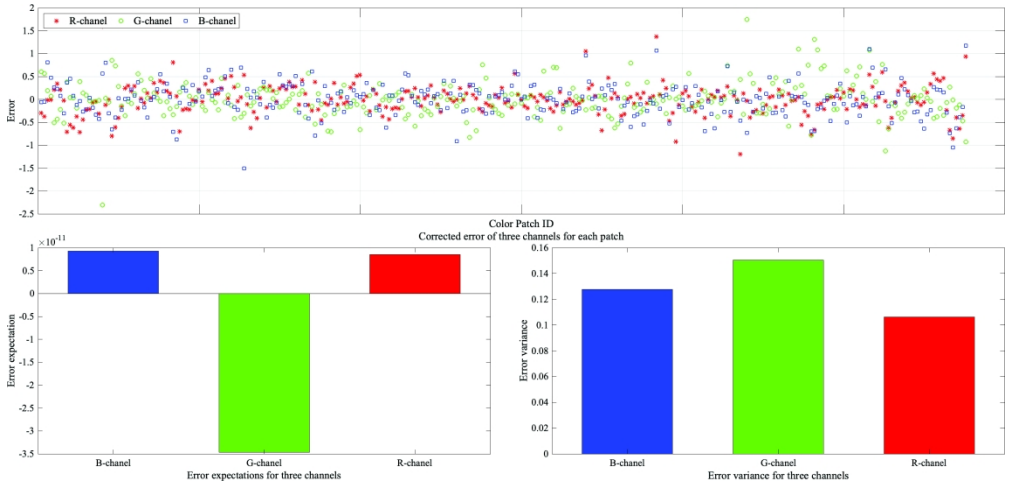

1011x482mm (600 x 600 DPI)

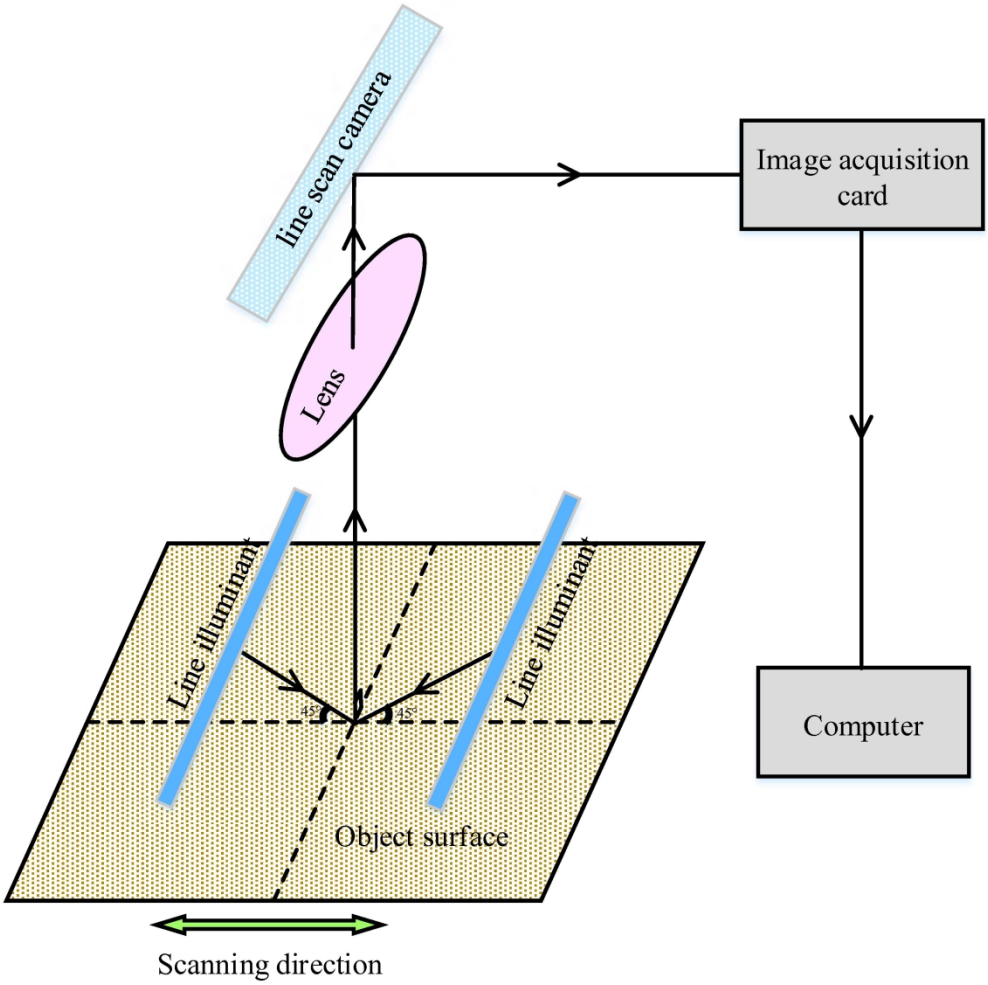

141x140mm (600 x 600 DPI)

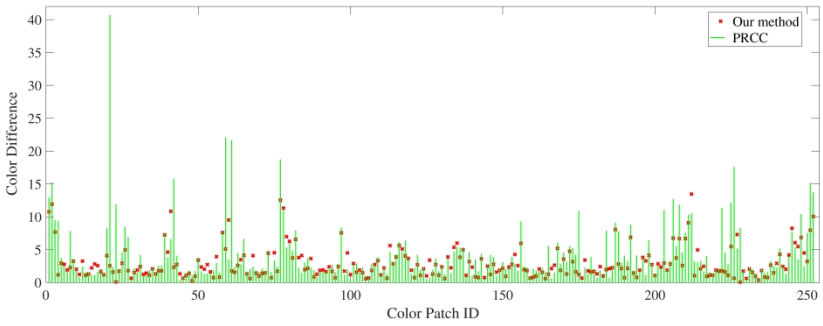

508x172mm (600 x 600 DPI)

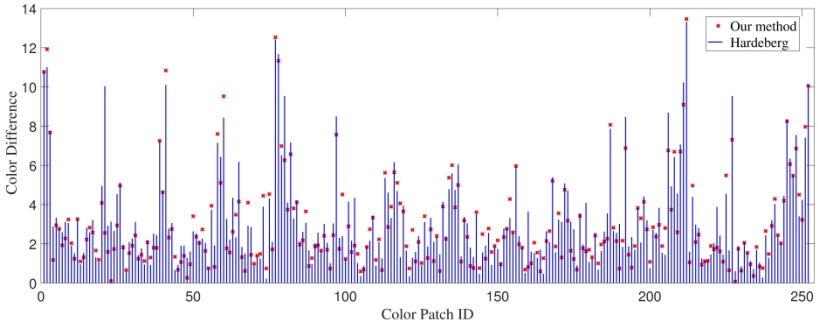

508x172mm (600 x 600 DPI)

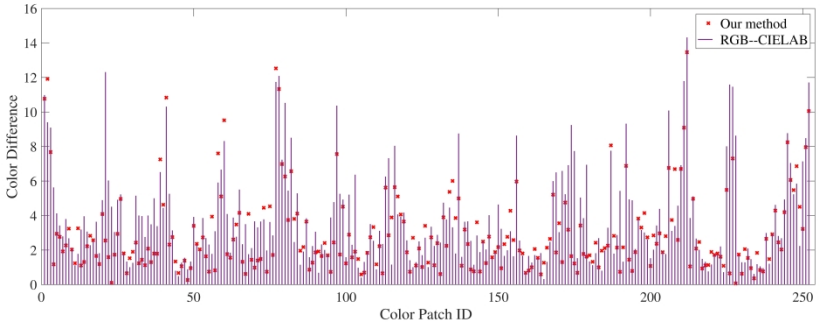

508x172mm (600 x 600 DPI)

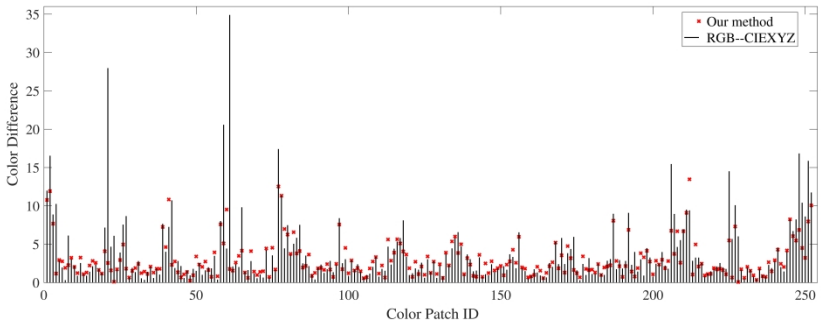

508x172mm (600 x 600 DPI)

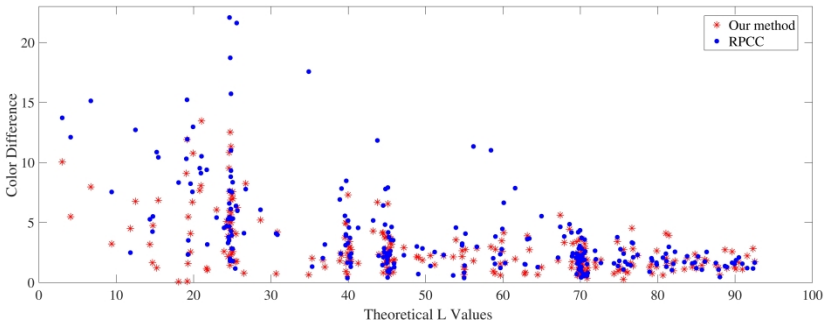

508x172mm (600 x 600 DPI)

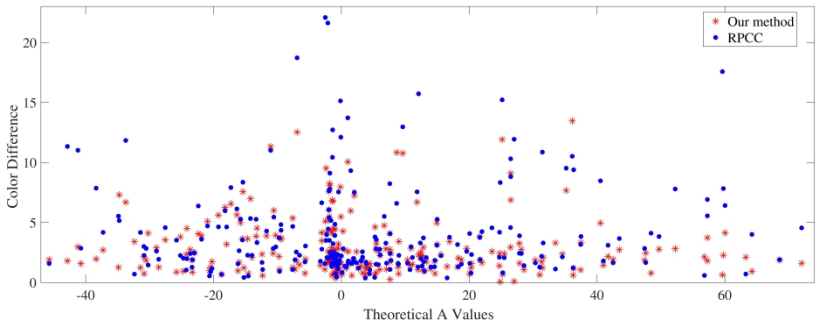

508x172mm (600 x 600 DPI)

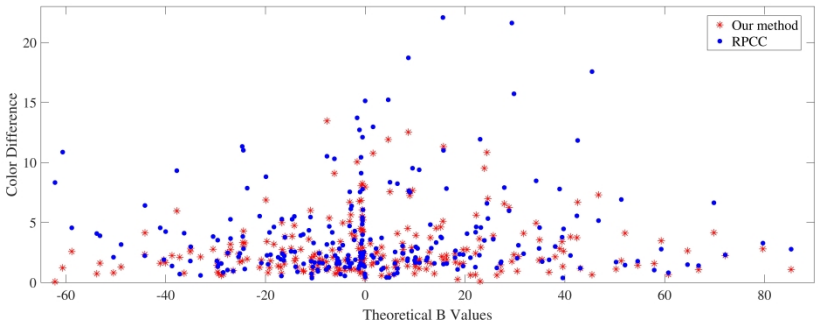

508x172mm (600 x 600 DPI)

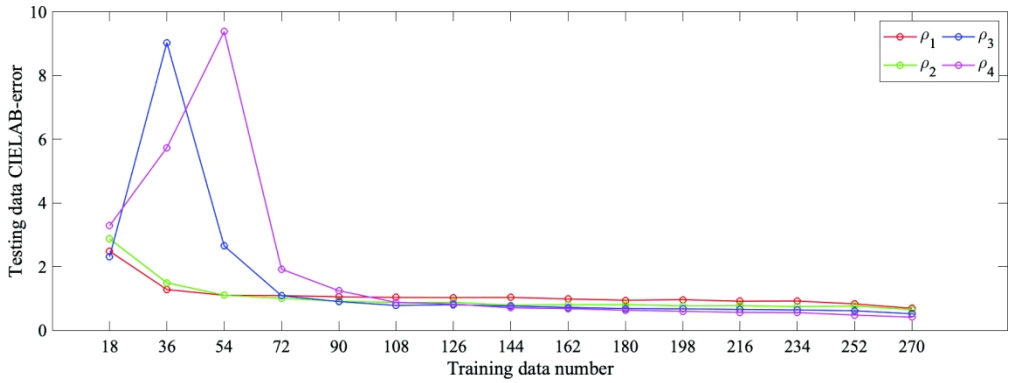

645x240mm (600 x 600 DPI)

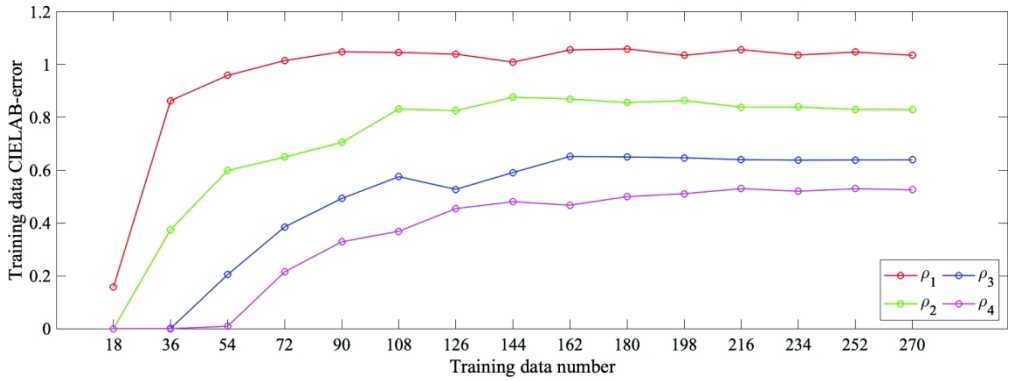

648x240mm (600 x 600 DPI)

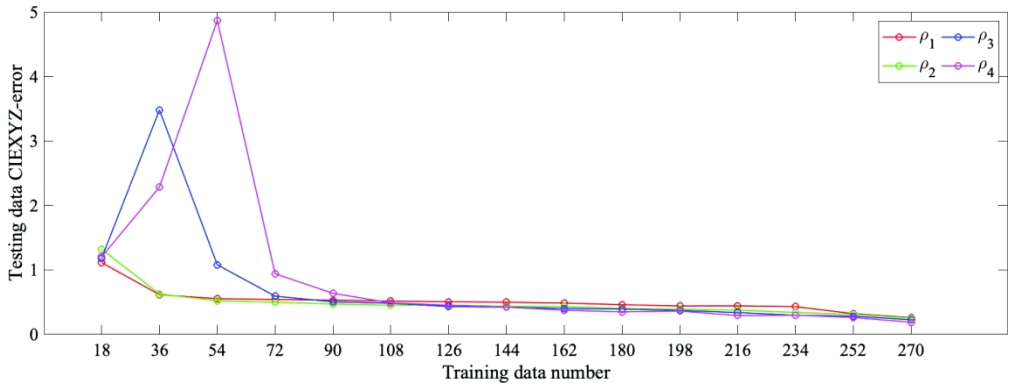

639x240mm (600 x 600 DPI)

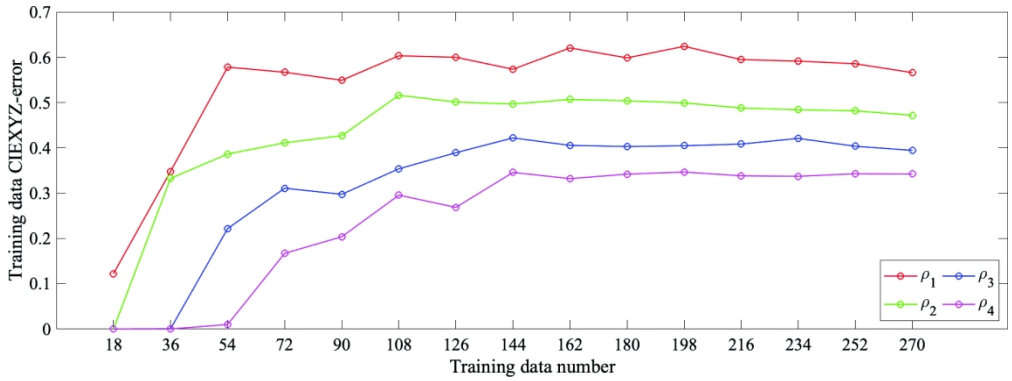

648x240mm (600 x 600 DPI)

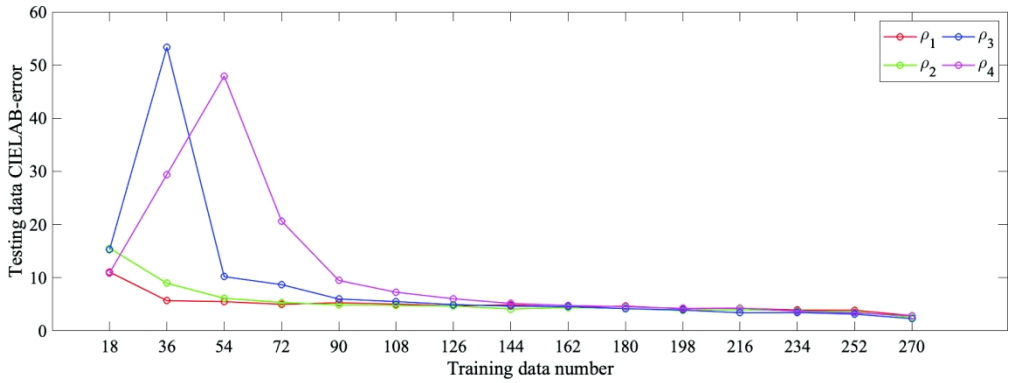

645x240mm (600 x 600 DPI)

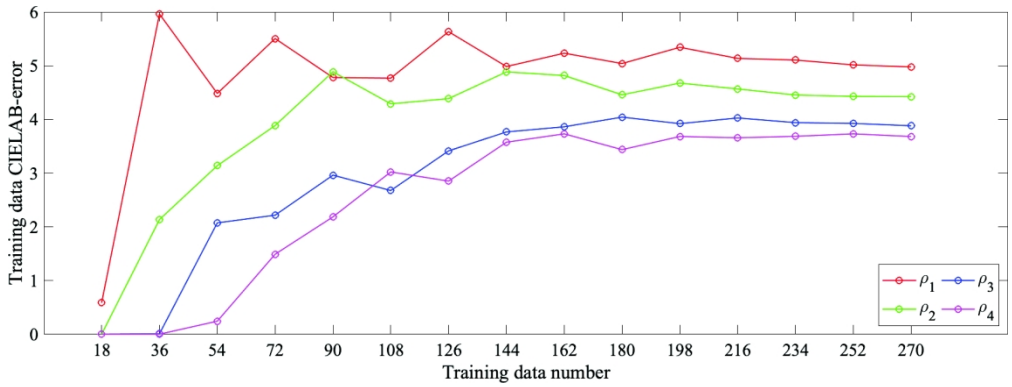

639x240mm (600 x 600 DPI)